Journal of Colloid and Interface Science **256,** 23–32 (2002)
doi:10.1006/jcis.2001.7821

# Adsorption of Ionic Surfactants on Solid Particles Determined by Zeta-Potential Measurements: Competitive Binding of Counterions

N. K. Dimov,* V. L. Kolev,* P. A. Kralchevsky,*,[1] L. G. Lyutov,# G. Broze,† and A. Mehreteab‡

**Laboratory of Chemical Physics & Engineering, Faculty of Chemistry, University of Sofia, 1164 Sofia, Bulgaria; #Department of Inorganic Chemistry, Faculty of Chemistry, University of Sofia, 1164 Sofia, Bulgaria; †Colgate–Palmolive R&D, Inc., Avenue du Parc Industriel, B-4041 Milmort (Herstal), Belgium; and ‡Colgate-Palmolive Technology Center, Piscataway, New Jersey 08854-5596*

Received March 18, 2001; accepted July 6, 2001; published online September 24, 2001

**A method for determining the equilibrium adsorption of an ionic surfactant on oppositely charged solid particles is proposed. Data from $\zeta$-potential measurements are processed to obtain the adsorption constants of surfactant ions and counterions. The method can be applied to particles of arbitrary size and shape, but only if their characteristic dimension is much larger than the thickness of the electric double layer. The adsorption is quantified solely by zeta-potential experiments; additional measurements of concentration depletion and specific particle-surface area are not needed. The approach is suitable for concentrations below the threshold of hemimicelle formation. We carried out experiments on adsorption of dodecyl-trimethyl-ammonium-bromide on glass particles in the presence of 1 mM NaBr. The particles were obtained by crushing a glass plate to powder and subsequent screening to remove particles larger than 20 $\mu$m. Control experiments with spherical particles from the same material showed that the method is insensitive to particle shape. Since the surfactant ($DTA^+$) and $Na^+$ bear the same electric charge, they compete with each other in the adsorption at the negatively charged glass. This is accounted for in the theoretical model. The binding of $Na^+$ counterions is found to play an essential role in the overall adsorption process.** 

*Key Words:* **adsorption; cationic surfactant; counterion binding; DTAB; electric double layer; electrophoresis; glass particles; solid–liquid interface; surface potential; $\zeta$-potential.**

## 1. INTRODUCTION

Three major groups of methods for studying surfactant adsorption at solid surfaces could be distinguished.

The first group is based on detecting the *depletion* of the bulk concentration due to the surfactant adsorption at the solid surface. Various techniques have been applied to measure the depletion effect: colorimetric titration methods (1–4), static (5–7) and dynamic (8) surface-tension experiments, UV spectroscopy (9–11), fluorescence (12), and high-pressure liquid chromatography (13) [see also studies cited in Ref. (2)]. The depletion method is applied with solid particles dispersed in the liquid phase. Consequently, to determine the surfactant adsorption one has also to measure the area of the solid–liquid interface per unit mass of the particles; the latter can be achieved by means of the BET–$N_2$ desorption method (9, 11), dynamic light scattering (6, 7), or electron microscopy (13).

The second group includes *direct* methods such as ellipsometry (14), neutron reflection (15–17), small-angle neutron scattering (18–20), NMR spectroscopy (21), total internal reflection sum-frequency spectroscopy (22, 23), and X-ray diffraction and atomic force microscopy (24) [see also Ref. (25)].

The third group consists of *electrokinetic* methods for studying the adsorption of ionic surfactants at solid surfaces. Such measurements can be accomplished with macroscopic surfaces by means of the flat-plate streaming potential apparatus (26–29), as well as with microscopic particles by using electrophoretic mobility measurements (2, 8, 10, 11, 30, 31).

It is important to note that not only surfactant ions but also common, nonamphiphilic ions can bind to a charged water–solid interface. The latter fact makes more difficult the interpretation of the measured $\zeta$-potentials. Nevertheless, in a previous work, Ref. (8), we succeeded in interpreting the pH-dependent binding of various ions to the head groups of adsorbed amphoteric surfactant using Stern adsorption isotherms combined with the theory of the electric double layer (EDL).

Our aim in the present paper seems somewhat simpler, viz., to determine the adsorption of an ionic surfactant on oppositely charged solid particles from the measured $\zeta$-potential. However, in contrast with Ref. (8), where monodisperse latex spheres were used, in the present study we carry out measurements with *polydisperse angular* particles. In other words, our purpose is to extend the method from Ref. (8) to a wider class of colloidal suspensions, including such containing particles with irregular shape and size distribution. In this respect, we utilize the fact that the microelectrophoretic measurements of $\zeta$-potential are not sensitive to the size and shape of the particles when the thickness of the EDL is much smaller than the characteristic particle diameter. The latter fact simplifies the experimental procedure because it is not necessary to determine the area of the solid–liquid interface per unit mass of the particles, as is needed for the

[1] To whom correspondence should be addressed. E-mail: pk@ltph.bol.bg.



0021-9797/02 $35.00

depletion method (see above). To verify whether or not the effect of the particle size and shape is really negligible, we carry out comparative experiments with angular and spherical particles of the same material (glass).

The paper is structured as follows. First we briefly present the theoretical background and obtain an appropriate equation for fitting the experimental plot of $\zeta$-potential vs surfactant concentration. Next, we describe the experimental procedures of preparation of particles, pretreatment of their surfaces, and $\zeta$-potential measurements. Further, we compare the theory and experiment, verify the numerical procedure, and discuss the results. The depletion effect is estimated and found negligible for the investigated diluted suspensions. This article demonstrates that the adsorption of an ionic surfactant at a solid surface can be quantified by $\zeta$-potential experiments alone (measurements of concentration depletion and specific particle-surface area are not necessary). The developed approach is suitable for the ion-exchange region of the Somasundaran-Fuerstenau adsorption isotherm (25, 32), (i.e., below the critical hemimicelle concentration).

## 2. THEORETICAL BACKGROUND

### 2.1. Physical System and Basic Equations

We consider the adsorption of an ionic surfactant at a solid surface, which exhibits ionizable surface groups of the opposite electric charge. An example is the system used in our experiments: adsorption of the cationic surfactant dodecyltrimethyl-ammonium-bromide (DTAB) at the water–glass interface (Fig. 1). The negative surface charge of glass is due to ionized silanol groups, $SiO^-$. In general, we assume that the aqueous solution contains not only dissolved surfactant, but also a nonamphiphilic electrolyte, NaBr in our experiments. In such cases, there is a competitive adsorption of the two kinds of counterions, $DTA^+$ and $Na^+$, in the Stern layer (33) (see Fig. 1). We denote the adsorptions of the amphiphilic and nonamphiphilic counterions in the Stern layer $\Gamma_1$ and $\Gamma_2$, respectively.

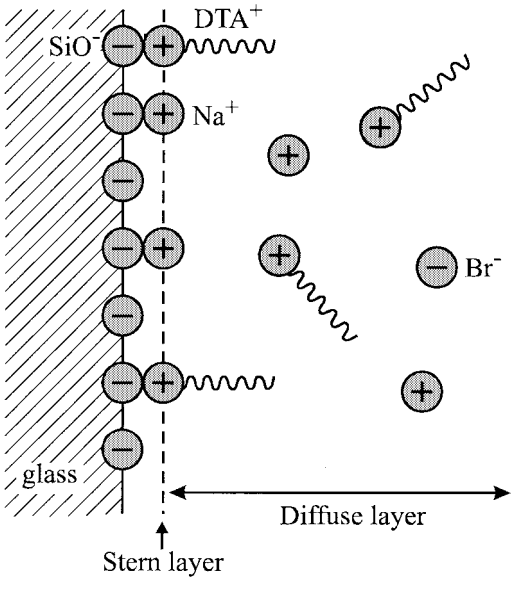


**FIG. 1.** Sketch of the electric double layer in a vicinity of a negatively charged solid (glass) surface in contact with aqueous solution of DTAB with added NaBr. The Stern layer consists of adsorbed (bound) counterions, whereas the diffuse layer contains free ions involved in Brownian motion.

**TABLE 1**
**Adsorption Isotherms**

| | |
|---|---|
| Henry | $K_i c_{is} = \dfrac{\Gamma_i}{\Gamma_s}, \quad i = 1, 2$ |
| Langmuir | $K_i c_{is} = \dfrac{\Gamma_i}{\Gamma_s - \Gamma}, \quad i = 1, 2$ |
| Frumkin | $K_i c_{is} = \dfrac{\Gamma_i}{\Gamma_s - \Gamma} \exp\left(-\dfrac{2\beta\Gamma}{kT}\right), \quad i = 1, 2$ |

*Note.* The notation $\Gamma = \Gamma_1 + \Gamma_2$ is used.

In our experiments the concentration of NaBr was kept constant at 1 mM, which corresponds to a characteristic thickness of the EDL, $\approx$3 nm. Since the latter value is much smaller than the particle size (from 2 to 15 $\mu$m; see below), in our theoretical analysis we consider a flat EDL.

From a formal thermodynamic viewpoint, the total adsorption of the counterions is (34–37)

$$\Gamma_i^{(\mathrm{tot})} = \Gamma_i + \Lambda_i \quad (i = 1, 2), \qquad [1]$$

where $\Lambda_i$ is the integral contribution of the diffuse part of the EDL:

$$\Lambda_i = \int_0^\infty [c_i(x) - c_{i\infty}]\, dx \quad (i = 1, 2). \qquad [2]$$

Here the $x$-axis is directed perpendicular to the solid surface (the latter is situated at $x = 0$), $c_{i\infty}$ is bulk concentration, and $c_i(x)$ is the variable concentration of the respective ionic species in the diffuse EDL. Below we focus our attention on the determination of $\Gamma_1$ and $\Gamma_2$ [i.e., on the counterion adsorption (binding) in the Stern layer].

It is known (25, 32, 38–40) that with the increase of surfactant concentration the surfactant adsorption at a solid–water interface exhibits several characteristic regions: (i) ion-exchange type adsorption at lower surfactant concentration; (ii) formation of hemimicelles (a cooperative effect) at higher concentrations; (iii) electrostatic hindrance of adsorption due to charge reversal; and (iv) saturated adsorption. In the present article we focus our attention on the region of ion-exchange (Fig. 1). In this case one can describe the adsorption of counterions in the Stern layer by using either of the isotherms shown in Table 1 [for details see, e.g., Refs. (37, 41)].

In Table 1 $\Gamma_s$ is the concentration of the adsorption sites (ionized groups) at the solid–water interface, $K_1$ and $K_2$ are adsorption constants for the two types of ions, $\beta$ is the interaction parameter in the Bragg–Williams statistical model (42), which

accounts for the interaction between the adsorbed counterions, and $c_{is} = c_i\,(x = 0)$ is the subsurface concentrations of the respective ionic species ($i = 1, 2$). Hereafter the potential of the Stern layer will be (approximately) identified with the $\zeta$ potential (this assumption is discussed in Section 6 below). Therefore, the subsurface and bulk concentrations, $c_{is}$ and $c_{i\infty}$, can be related by means of the Boltzmann equation (43)

$$c_{is} = c_{i\infty} \exp\left(-\frac{e\zeta}{kT}\right) \quad (i = 1, 2), \qquad [3]$$

where $e$ is the absolute value of the electron charge, $k$ is the Boltzmann constant, and $T$ is the temperature.

For negligible interaction between the adsorbed species ($\beta \to 0$) the Frumkin isotherm (44) reduces to the Langmuir isotherm (45); the latter reduces to the Henry isotherm in the case of low adsorption, $\Gamma_i \ll \Gamma_s$ (see Table 1). Note that the Langmuir isotherm, applied to the binding of ionic species, is often termed the Stern isotherm (46). Note also that the adsorption constant $K_i$ is related to the standard free energy of counterion adsorption (binding) $\Delta\mu_i^{(0)}$ by the equation (25, 47)

$$K_i = \frac{\delta_i}{\Gamma_s} \exp\left(\frac{\Delta\mu_i^{(0)}}{kT}\right) \quad (i = 1, 2), \qquad [4]$$

where $\delta_i$ is the effective diameter of the respective ion.

The basis of the theoretical interpretation of the data from the $\zeta$-potential measurements is the known Gouy equation (46, 48), which relates the surface charge and potential; the version of this equation for an aqueous solution, containing 1 : 1 electrolyte (surfactant + salt), reads (37)

$$\Gamma_s - \Gamma_1 - \Gamma_2 = 4I\kappa^{-1} \sinh\left(\pm\frac{e\zeta}{2kT}\right), \qquad [5]$$

where the sign is plus or minus depending on whether the ionized surface groups bear, respectively, positive or negative surface charge. The sign must be minus for the system in Fig. 1. $\kappa$ is the Debye parameter and $I$ is the ionic strength of the solution

$$\kappa^2 = \frac{8\pi e^2 I}{\varepsilon kT}, \quad I = c_{1\infty} + c_{2\infty}. \qquad [6]$$

As already mentioned, in our experiments the ionic strength was fixed to $I = 10$ mM by the added NaBr.

### 2.2. Langmuirian Adsorption

Here we apply the Langmuir isotherm to describe the adsorption of surfactant and salt counterions at a solid–water interface in the "ion-exchange" regime (before the appearance of hemimicelles). Summing up the respective expressions in Table 1, for $i = 1$ and $i = 2$, one obtains

$$K_1 c_{1s} + K_2 c_{2s} = \Gamma/(\Gamma_s - \Gamma), \qquad [7]$$

where $\Gamma = \Gamma_1 + \Gamma_2$. Equation [7] can be rearranged in the form

$$\Gamma_s + E_1 c_{1s} + E_2 c_{2s} = \Gamma_s^2/(\Gamma_s - \Gamma). \qquad [7a]$$

We have introduced the notation

$$E_i = \Gamma_s K_i = \delta_i \exp\left(\frac{\Delta\mu_i^{(0)}}{kT}\right) \quad (i = 1, 2). \qquad [8]$$

Next, it is convenient to express the Gouy equation, Eq. [5], in the form

$$\Gamma_s - \Gamma = \Gamma_0 \sinh(\tilde{\zeta}/2), \qquad [9]$$

where

$$\tilde{\zeta} = \frac{e|\zeta|}{kT}, \quad \Gamma_0 = 4I\kappa^{-1}. \qquad [10]$$

In terms of the same notation, Eq. [3] acquires the form

$$c_{is} = c_{i\infty} \exp(\tilde{\zeta}) \quad (i = 1, 2). \qquad [11]$$

Finally, we substitute Eq. [9] into the right-hand side of Eq. [7a]; after some transformations, we obtain

$$c_{1s} = C\left[\frac{\tilde{\Gamma}_s^2}{\sinh(\tilde{\zeta}/2)} - \tilde{\Gamma}_s - A\exp(\tilde{\zeta})\right], \qquad [12]$$

where we have introduced the notation

$$\tilde{\Gamma}_s = \frac{\Gamma_s}{\Gamma_0}, \quad A = \frac{E_2 c_{2\infty}}{\Gamma_0}, \quad C = \frac{\Gamma_0}{E_1}. \qquad [13]$$

$\tilde{\Gamma}_s$ and $A$ are dimensionless parameters, whereas $C$ has a dimension of concentration.

In the experiment one obtains data for $\zeta$ vs $c_{1\infty}$ (see below), which can be easily transformed into a set of data for $c_{1s}$ vs $\tilde{\zeta}$ with the help of Eqs. [10] and [11]. The latter set of data can be processed by means of the theoretical dependence, Eq. [12]; the parameters $\tilde{\Gamma}_s$, $A$, and $C$ are to be determined from the best fit. With this end in view, below we describe the experiment.

## 3. EXPERIMENT

### 3.1. Preparation of the Particles

In most of our experiments we used particles obtained by simply crushing a glass plate into powder. A fine fraction of glass powder (size $\leq 20$ $\mu$m) was collected by means of a sieve. Such particles have angular shape (see Fig. 2a).

Insofar as the thickness of the double electric layer is much smaller than the characteristic particle size, one can expect that the measured $\zeta$ potential is not sensitive to the size and shape of the angular glass particles [see, e.g., Ref. (47)]. To check this

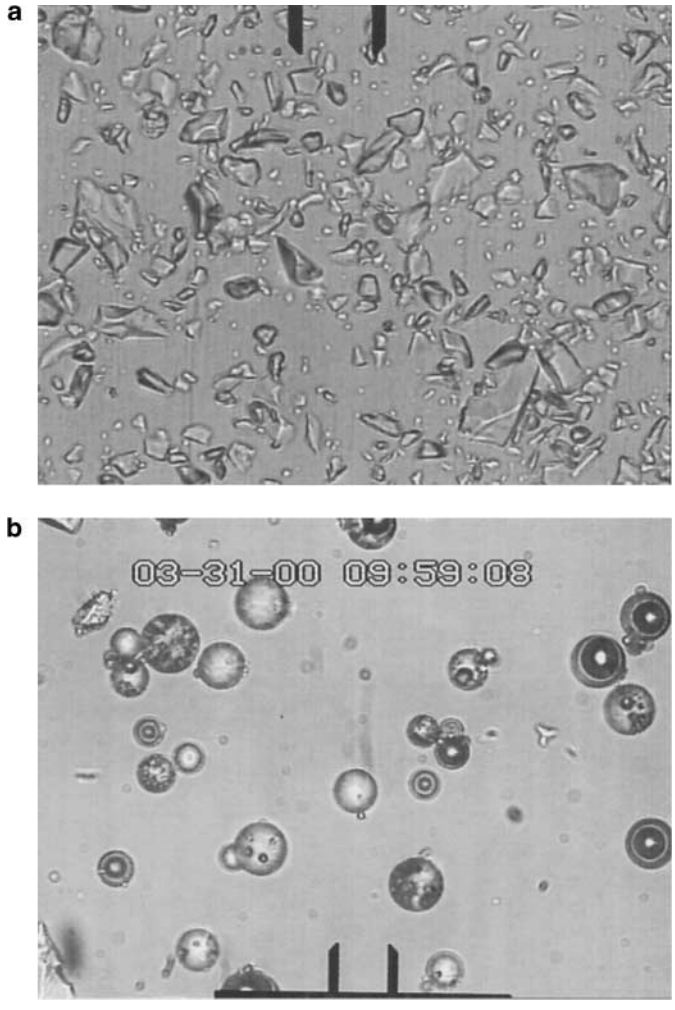


**FIG. 2.** Photographs of (a) rough glass particles (powder) passed through a 20-$\mu$m sieve; and (b) almost spherical glass particles obtained by melting the former particles in a burning gas flow (see Fig. 3). The reference distances are (a) 20 $\mu$m and (b) 10 $\mu$m.

expectation, we also carried out control experiments with particles of *the same* material, but with spherical shape and known size distribution. The spherical glass particles (Fig. 2b) were prepared in the following way.

The fine glass powder (angular particles, size $\leq 20$ $\mu$m) was introduced into a gas flow (propane–butane + oxygen) and heated quickly to about 2000°C as a result of the burning of the gas mixture. At that temperature the angular particles melted and transformed into small spheres. Then the particles were cooled quickly (for ca. 0.01 s) in the raising gas flow; as a result they solidified and stuck to the inner walls of the working chamber (Fig. 3). Finally, the particles were gently detached from the walls, washed, dried, and stored as a suspension in water for use in the experiment. Figure 2b shows the rounded (almost spherical) particles obtained in this way. By microscopic observations of these "spherical" particles and semiautomatic image analysis, we determined their size histogram (Fig. 4), which is close

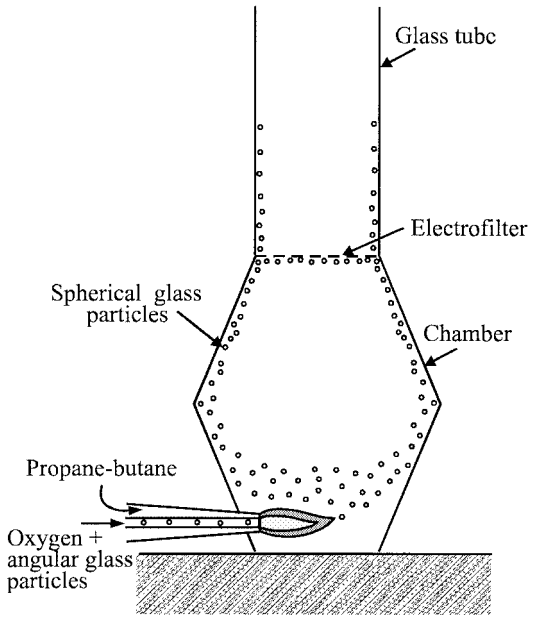


**FIG. 3.** Sketch of the experimental setup for the preparation of spherical glass particles by melting the glass powder in the flame of burning propane–butane (see the text for details).

to the log-normal distribution. The average diameter of these particles is

$$2R = 5.6\ \mu\text{m}. \qquad [15]$$

### 3.2. *Treatment of the Particles*

To unify the surface properties of the particles, they were subjected to the following treatment. A portion of particles, of weight $\leq$10 g, was placed in a glass beaker filled with 20 ml water, and then 5 g $KClO_4$ was added. Next, about 30 ml concentrated $H_2SO_4$ was poured into the beaker. The mixture was kept at room temperature for about 2 h. After that, the acid was diluted with 500 ml pure (milliQ) water and the particles were allowed to sediment at the bottom of the beaker. The acidic

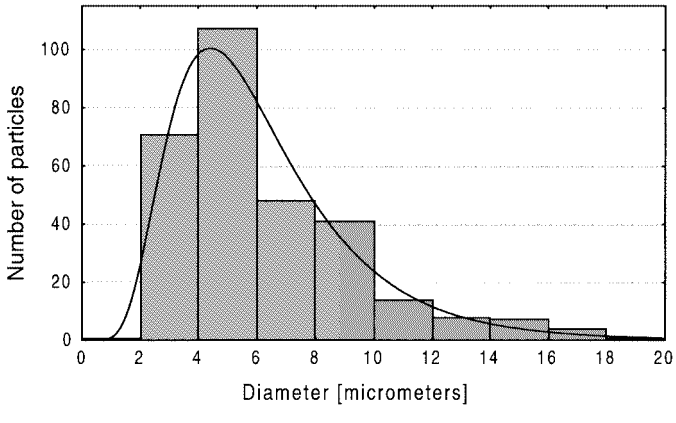


**FIG. 4.** Experimental size-distribution histogram for the spherical glass particles (Fig. 2b).

aqueous phase was removed and the particles were washed several times with pure water. Finally, they were dried at $T \approx 100°C$, until their mass remained constant (complete water evaporation), and were used further in the experiment.

The above treatment leads to an increase in the surface density of Si–O–Si and SiOH groups at the cost of a decreased density of the charged surface groups, $SiO^-$. The glass is an alkali silicate; after its reduction to fine particles, the obtained aqueous suspension exhibits a basic pH. The applied treatment with $H_2SO_4$ removes the alkali reaction of the suspension. This treatment removes also organic impurities (if any). Indeed, the mixing of $KClO_4$ with $H_2SO_4$ produces perchloric acid ($HClO_4$), which is able to oxidize the organic impurities.

### 3.3. $\zeta$-Potential Measurements: Experimental Procedure

As already mentioned, the surfactant and salt in our experiments were DTAB and NaBr, both of them from Sigma. The working concentration of NaBr was fixed to $c_{2\infty} = 10$ mM. This salt concentration is appropriate for the electrophoretic $\zeta$-potential measurements and keeps constant the ionic strength of the solution, $I$, insofar as $c_{2\infty} \gg c_{1\infty}$ in our experiments. To prepare samples for the $\zeta$-potential experiments we applied the following procedure.

A weighted amount of glass particles was added to 100 ml 10 mM aqueous NaBr solution and agitated for 2 h by magnetic stirrer. The experimental concentrations of the glass particles in the used suspensions were as follows;

$$\varphi_m = \begin{cases} 0.077\ \text{g/cm}^3\ \text{(angular particles)} \\ 0.070\ \text{g/cm}^3\ \text{(spherical particles)} \end{cases}. \qquad [16]$$

Next, a sample of several milliliters was taken from the suspension to measure the $\zeta$ potential of the particles. Then a specified small amount (<1 ml) of a stock aqueous DTAB solution was added to the suspension. The agitation was continued and 2 h later the next sample was taken from the suspension to measure $\zeta$. After the addition of a subsequent portion of DTAB solution, the procedure was repeated until the suspension was spent.

In the $\zeta$-potential measurements, by means of "Malvern Zetasizer IIc," we used small portions (about 5 ml) of the suspensions. Some illustrative experimental values are shown in Table 2. The negative sign of $\zeta$, and its relatively weak dependence on $c_{1\infty}$, indicate that in the investigated case the adsorption of $DTA^+$ ions on glass happens in the ion-exchange regime. The results for the two types of particles are plotted in Figs. 5a and 5b as $\zeta$ vs $c_{1s}$. An examination of the data shows that the values of $|\zeta|$ are systematically slightly greater for the spherical particles compared to the angular ones. This small difference might be due to the difference between the shapes of the two types of glass particles, but it could be also a manifestation of some delicate difference between their surface properties induced by the pretreatment (unlike the angular particles, the spherical ones were subjected to melting; see Fig. 3). The experimental data are interpreted in the next section.

**TABLE 2**
**Experimental Data for the $\zeta$-Potential of Glass Particles**

| Spherical glass particles | | Angular glass particles | |
|---|---|---|---|
| $c_{1\infty}$ (mM) | $\zeta$ (mV) | $c_{1\infty}$ (mM) | $\zeta$ (mV) |
| 0 | −44.2 | 0 | −41.7 |
| 0.097 | −43.8 | 0.14 | −39.0 |
| 0.36 | −39.5 | 0.35 | −36.2 |
| 0.66 | −36.5 | 0.41 | −35.4 |
| 0.89 | −33.2 | 0.77 | −30.0 |

*Note.* $c_{1\infty}$ is the total input concentration of DTAB in the suspension; the concentration of added NaBr is always 10 mM.

## 4. INTERPRETATION OF THE EXPERIMENTAL RESULTS

### 4.1. Comparison of Theory and Experiment

Our purpose in this section is to process the experimental data in order to determine $\Gamma_1$ and $\Gamma_2$ (i.e., the adsorptions of $DTA^+$

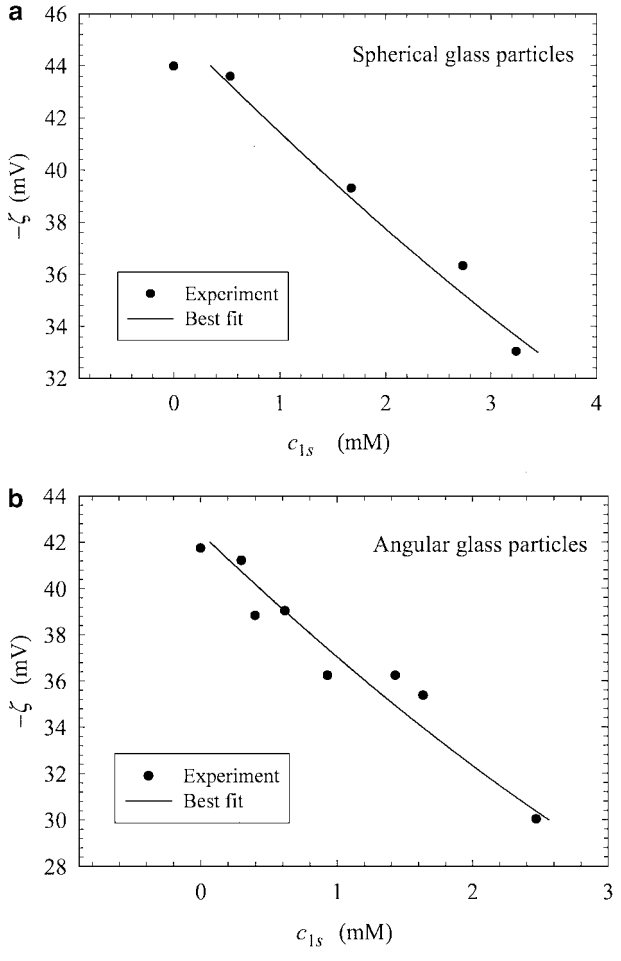


**FIG. 5.** Plots of the experimental data for the $\zeta$-potential vs the subsurface concentration $c_{1s}$ of $DTA^+$ ions (see Eq. [3]). The lines are the best fits with Eq. [12] for (a) spherical and (b) angular glass particles (see Table 3 for the determined parameters).

and $Na^+$ at the negatively charged glass surface) as functions of the surfactant concentration. In our experiments the bulk concentration of $DTA^+$, $c_{1\infty}$, is increased at fixed concentration of $Na^+$, $c_{2\infty}$, but in all cases we have $c_{1\infty} \ll c_{2\infty}$. Nevertheless, we detect a decrease in the magnitude of $\zeta$ with about 28% (Table 2). This fact implies that the adsorption (binding) energy of $DTA^+$ is greater than that of $Na^+$, viz., $\Delta\mu_1^{(0)} > \Delta\mu_2^{(0)}$ (see Eq. [4]); in other words, $DTA^+$ is able to replace $Na^+$ from the Stern layer.

We use Eq. [12] to fit the experimental data (Fig. 5). Equation [12] contains three parameters, $C$, $\tilde{\Gamma}_s$, and $A$. If one has a sufficient number of experimental points, one can determine all three parameters from the best fit. Alternatively, one could estimate $A$ from another set of data and use only $C$ and $\tilde{\Gamma}_s$ as adjustable parameters.

Assuming (approximately) equal energies of binding of $Na^+$ to $O^-$ in the –(OSi)–$O^-$ and –($O_3$S)–$O^-$ groups, we take values determined in Ref. (37) for the binding of $Na^+$ to the head groups of sodium dodecyl sulfate (SDS) adsorption monolayers, viz., $\Delta\mu_2^{(0)}/kT = 1.64$ and $\delta_2 = 0.7$ nm. With these parameter values from Eq. [8] one estimates $E_2 \approx 3.61$ nm. Next, having in mind that $I \approx c_{2\infty} = 0.01$ M, with the help of Eqs. [6], [10], and [13] we estimate

$$\Gamma_0 \approx 7.304 \times 10^{12}\ \mathrm{cm}^{-2}, \quad A \approx 0.2975. \qquad [17]$$

Further, the parameters $C$ and $\tilde{\Gamma}_s$ are determined from the best fit of the experimental data as follows. Following the least-squares method, we consider the merit function

$$\Phi(C, \tilde{\Gamma}_s) = \sum_{k=1}^{N} \left[c_{1s}^{(k)} - c_{1s}\left(\zeta^{(k)}, C, \tilde{\Gamma}_s\right)\right]^2, \qquad [18]$$

where the summation is carried out over all experimental points $(c_{1s}^{(k)}, \zeta^{(k)})$, whose number is denoted by $N$; the function $c_{1s}(\zeta^{(k)}, C, \tilde{\Gamma}_s)$ is defined by Eq. [12]. Note that $c_{1s}^{(k)}$ is calculated from the experimental $c_{1\infty}^{(k)}$ and $\zeta^{(k)}$ by means of Eq. [3]. In our computations we applied a numerical minimization of the function $\Phi$ in an appropriately chosen two-dimensional number domain $(C, \tilde{\Gamma}_s)$. The minimum of $\Phi$ corresponds to the best fit; the respective values of $C$ and $\tilde{\Gamma}_s$ are listed in Table 3 for the data in Figs. 5a and 5b. Next, we calculate the density of the adsorption sites on the glass surface, $\Gamma_s$, and the adsorption (binding) energy of $DTA^+$ to glass, $\Delta\mu_1^{(0)}$, using Eqs. [8], [13], and [17] with $\delta_1 \approx 2$ nm; the results are given in Table 3.

**TABLE 3**
**Parameters Related to the Adsorption of $DTA^+$ at a Glass Surface**

| Type of particles | $\tilde{\Gamma}_s$ | $C$ (mM) | $\Gamma_s^{-1}$ (nm$^2$) | $\frac{\Delta\mu_1^{(0)}}{kT}$ |
|---|---|---|---|---|
| Spherical | $1.91 \pm 0.24$ | $1.47 \pm 0.35$ | $7.15 \pm 0.89$ | $3.73 \pm 0.24$ |
| Angular | $1.74 \pm 0.25$ | $1.16 \pm 0.33$ | $7.87 \pm 1.15$ | $3.96 \pm 0.28$ |

*Note.* Results from the best fits of the data in Figs. 5a and 5b with Eq. [12].

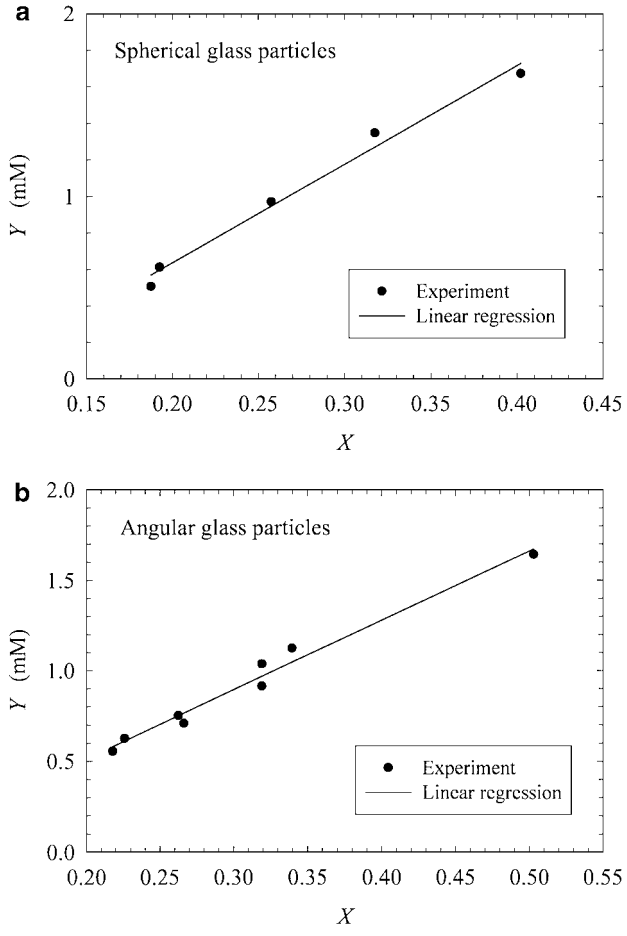


**FIG. 6.** Plots of the experimental data in accordance with Eqs. [19] and [20]: (a) spherical and (b) angular glass particles (see the text for details).

### *4.2. Verification of the Numerical Procedure and Discussion*

Equation [12] can be represented in the form

$$Y = BX + D, \qquad [19]$$

where

$$X = \frac{\exp(-\tilde{\zeta})}{\sinh(\tilde{\zeta}/2)}, \quad Y = (c_{1s} + C\tilde{\Gamma}_s)\exp(-\tilde{\zeta}), \qquad [20]$$

$$B = C\tilde{\Gamma}_s^2, \quad D = AC. \qquad [21]$$

In Figs. 6a and 6b we have plotted the same data as in Figs. 5a and 5b, but now as $Y$ vs $X$. Note that to calculate $C\tilde{\Gamma}_s$ in the expression for $Y$ we use values from Table 3, which have been determined by using a nonlinear fit (see Eq. [18]). The straight lines in Fig. 6 are the best fits of the data with a linear regression, in accordance with Eq. [19]. The use of this secondary linear fit is the following. (i) From the agreement between the data points and the straight line (Figs. 6a and 6b), one can judge about the adequacy of the theoretical model. (ii) The standard computer

programs for linear regression give automatically the errors of the slope and the intercept, $B$ and $D$ in Eq. [19], from which one can easily estimate the experimental error of the parameters $C$ and $\tilde{\Gamma}_s$ by using Eq. [21]. The standard deviations of the values shown in Table 3 are estimated in this way.

In our case, the values of $C$ and $\tilde{\Gamma}_s$ determined from the linear fits (Fig. 6) agree well with those obtained from the basic nonlinear fit (Fig. 5). Moreover, having in mind the experimental error, the values in Table 3 for spherical and angular particles are close to each other (practically coincident in the framework of the experimental accuracy). This result confirms our expectations that the effect of the different particle shape is negligible; note that $\kappa^{-1} = 3.03$ nm, whereas the particle size is from 2 to 15 $\mu$m. The relatively low density of the ionized surface groups of glass, $\Gamma_s^{-1} = 7$–$8$ nm$^2$ per surface charge, can be attributed to the pretreatment with $KClO_4$ and $H_2SO_4$, and heating (see Section 3.2). As expected, the adsorption energy of $DTA^+$ ions, $\Delta\mu_1^{(0)} \approx 3.8\,kT$, is larger than that of the $Na^+$ ions, $\Delta\mu_2^{(0)} \approx 1.64\,kT$. Nevertheless, the adsorption (binding) of the $Na^+$ ions is considerable owing to their comparatively large bulk concentration in the solution.

For an air–water interface the surfactant adsorption is accompanied with a free-energy gain owing to the transfer of the *hydrocarbon tail* out of the aqueous phase. In this case the values of $\Delta\mu_1^{(0)}$ are typically in the range of 10–14 $kT$ (25–35 kJ/mol) [see, e.g., Refs. (37, 49)]. In the present case, the lower value $\Delta\mu_1^{(0)} \approx 3.8\,kT$ is related to the fact that the $DTA^+$ ion adsorbs with its *head group* to the solid surface, the hydrocarbon tail remaining all the time in aqueous environment. Then, two oppositely directed effects are expected to influence $\Delta\mu_1^{(0)}$. (i) The quaternary ammonium of the $DTA^+$ ion is surrounded by three $-CH_3$ groups, which may increase the distance between the positive charge of the surfactant head group and the negative surface charge of the glass substrate; this tends to decrease $\Delta\mu_1^{(0)}$. (ii) The head group of $DTA^+$ is expected to be less hydrated than that of $Na^+$; this would lead to a shorter distance between the plus charge of the surfactant and the minus charge of the solid surface, and consequently, would increase $\Delta\mu_1^{(0)}$. It seems that the latter effect is predominant, insofar as $\Delta\mu^{(0)}$ is greater for $DTA^+$ in comparison with $Na^+$.

### 4.3. Adsorptions of $DTA^+$ and $Na^+$ Ions

Once the parameters in Eq. [12] have been determined, one can calculate the adsorption isotherm, $\Gamma_1$ vs $c_{1\infty}$. With the help of Eqs. [8], [9], [11], and [13] one can bring Eq. [12] and the Langmuir isotherm in Table 1 (for $i = 1$) into the form

$$c_{1\infty}(\tilde{\zeta}) = C F(\tilde{\zeta}) \exp(-\tilde{\zeta}), \qquad [22]$$

$$\Gamma_1(\tilde{\zeta})/\Gamma_s = \Gamma_s^{-2} F(\tilde{\zeta}) \sinh(\tilde{\zeta}/2), \qquad [23]$$

where

$$F(\tilde{\zeta}) = \frac{\tilde{\Gamma}_s^2}{\sinh(\tilde{\zeta}/2)} - \tilde{\Gamma}_s - A\exp(\tilde{\zeta}). \qquad [24]$$

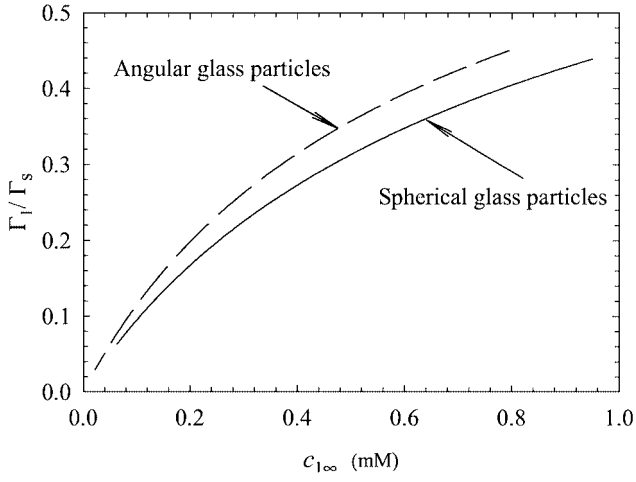


**FIG. 7.** Adsorption isotherm, $\Gamma_1/\Gamma_s$ vs $c_{1\infty}$, of surfactant ($DTA^+$) ions on glass calculated from Eqs. [22]–[23] using the experimental parameters in Table 3 for angular and spherical particles, for which $\Gamma_s^{-1} = 7.9$ and 7.2 nm$^2$, respectively.

The values of the parameters $A$, $C$, and $\tilde{\Gamma}_s$ are given by Eq. [17] and Table 3. Equations [22] and [23] represent the dependence $\Gamma_1(c_{1\infty})$ in a parametric form. The calculated curves $\Gamma_1(c_{1\infty})$, for the adsorption of $DTA^+$ on spherical and angular particles (using the parameters in Table 3), are plotted in Fig. 7. In fact, $\Gamma_1/\Gamma_s$ is the occupancy of the Stern layer (Fig. 1) with surfactant ($DTA^+$) ions. As could be expected, $\Gamma_1/\Gamma_s$ increases with the rise of the bulk concentration of DTAB (Fig. 7), which leads (i) to an exchange of $Na^+$ with $DTA^+$ in the Stern layer and (ii) to an increase in the total occupancy, $(\Gamma_1 + \Gamma_2)/\Gamma_s$, because of the higher adsorption energy of the $DTA^+$ ions ($\Delta\mu_1^{(0)} > \Delta\mu_2^{(0)}$).

Likewise, with the help of Eqs. [8], [9], [11], and [13] one can express the Langmuir isotherm in Table 1 for $i = 2$ in the form

$$\Gamma_2(\tilde{\zeta})/\Gamma_s = A\,\Gamma_s^{-2}\exp(\tilde{\zeta})\sinh(\tilde{\zeta}/2). \qquad [25]$$

Equations [22] and [25] determine the dependence $\Gamma_2(c_{1\infty})$ in a parametric form. Using $A$ from Eq. [17] and the parameters in Table 3 we calculate the isotherms $\Gamma_2(c_{1\infty})$ for spherical and angular particles (see Fig. 8). One sees that $\Gamma_2/\Gamma_s$ decreases with the increase of $c_{1\infty}$ at fixed $c_{2\infty}$, that is the binding of $Na^+$ ions decreases when the bulk concentration of DTAB is increased at fixed concentration of NaBr. As already mentioned, this decrease of $\Gamma_2/\Gamma_s$ is due to the replacement of the $Na^+$ by $DTA^+$ in the Stern layer (cf. Figs. 7 and 8). Indeed, it is seen that with the increase of $c_{1\infty}$ from 0 to 0.9 mM, $\Gamma_1/\Gamma_s$ increases from 0 to 0.45, whereas $\Gamma_2/\Gamma_s$ decreases from 0.45 to 0.20. The latter fact shows that the role of the $Na^+$ ions in the overall adsorption process is considerable and should not be neglected.

The total occupancy of the Stern layer, $(\Gamma_1 + \Gamma_2)/\Gamma_s$, rises from ca. 0.45 to 0.65. For comparison, the occupancy varies between 0.15 and 0.74 in the case of binding of $Na^+$ ions to the head groups of a SDS adsorption layer [see Ref. (37) and references therein]. Hence, in both cases the binding of counterions is well pronounced.

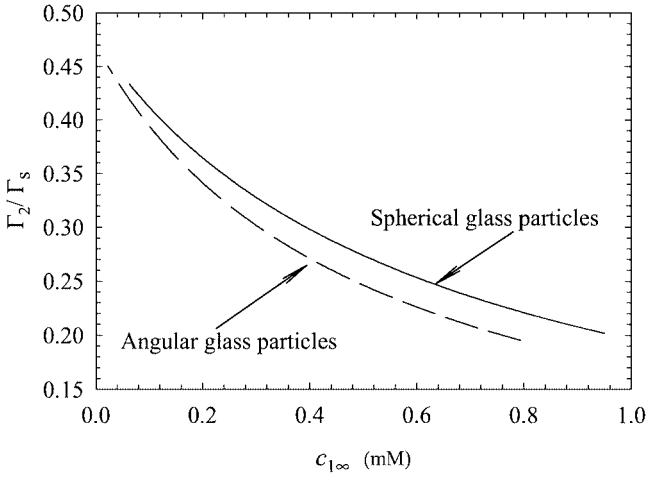


**FIG. 8.** Occupancy of the Stern layer with bound $Na^+$ ions, $\Gamma_2/\Gamma_s$, vs the bulk surfactant (DTAB) concentration, $c_{1\infty}$. Curves calculated from Eqs. [22] and [25] using the experimental parameters in Table 3 for angular and spherical glass particles; $\Gamma_s$ is the same as in Fig. 7.

With the values of $\Gamma_s$ and $\Delta\mu_1^{(0)}$ in Table 3, and $\delta_1 \approx 2$ nm, one can calculate the surfactant adsorption constant using Eq. [4]; the result is $K_1 = 359$ and 497 $M^{-1}$ for spherical and angular particles, respectively. Since in our experiments $c_{1s}$ can be $\geq 3 \times 10^{-3}$ M (see Fig. 5), the product $K_1 c_{1s}$ is not always much less than 1; in such cases the Langmuir isotherm cannot be linearized to reduce to the Henry isotherm. This confirms the adequacy of using the Langmuir isotherm in our theoretical model.

## 5. ESTIMATE OF THE DEPLETION EFFECT

After inserting the particles in the solution, the surfactant adsorbs at their surfaces, which leads to a decrease of the bulk surfactant concentration with

$$\Delta c \equiv c_{\text{tot}} - c_{1\infty}. \qquad [26]$$

Here $c_{\text{tot}}$ is the total input surfactant concentration and $c_{1\infty}$ stands for the residual surfactant concentration in the aqueous phase after the adsorption. On the other hand, one can write

$$\Delta c \equiv a_m \varphi_m \Gamma_1, \qquad [27]$$

where $a_m$ is the total area of the water–solid interface per unit mass of particles and $\varphi_m$ is given by Eq. [16] for the suspensions used in our experiments. Further, for spherical particles, $a_m$ can be expressed in the form

$$a_m = \frac{4\pi R^2 N}{\frac{4}{3}\pi R^3 \rho N} = \frac{3}{R\rho}, \qquad [28]$$

where $N$ is the number of particles, $R$ is their average radius, and $\rho$ is their mass density. Combining Eqs. [27] and [28] one obtains

$$\Delta c = C_p \frac{\Gamma_1}{\Gamma_s}, \quad C_p = \frac{3\varphi_m \Gamma_s}{R\rho}. \qquad [29]$$

Thus, for our spherical glass particles, using the values $\varphi_m = 0.070$ g/cm$^3$, $R \approx 3$ $\mu$m, $\Gamma_s^{-1} = 7.15$ nm$^2$, and $\rho = 2.6$ g/cm$^3$, one calculates $C_p = 6.25 \times 10^{-6}$ M. With this value of the coefficient $C_p$ one estimates

$$0 \leq \Delta c \leq 2.8 \times 10^{-6}\ \text{M} \qquad [30]$$

for the data in Fig. 7. In other words, $\Delta c/c_{1\infty} < 0.01$ (see the values of $c_{1\infty}$ in Table 2); a similar estimate holds also for the angular particles. The latter fact confirms that we can determine the surfactant adsorption on glass particles with the help of plots, such as those in Figs. 5a and 5b, with $c_{1\infty} \approx c_{\text{tot}}$. This simplification of the data analysis is achieved by merely keeping the input concentration of particles, $\varphi_m$, sufficiently low (cf. Eq. [16]), but still high enough to allow electrophoretic measurements of the $\zeta$ potential.

## 6. DISCUSSION

To determine the surfactant adsorption $\Gamma_1$ from the electrophoretic measurements, we assumed that the $\zeta$ potential is approximately equal to the $\psi_d$ potential of the Stern layer (Fig. 1). Below we discuss the consequences of this assumption.

The difference between $\zeta$ and $\psi_d$ has been a subject of many discussions in the literature (50, 51). In general, it is accepted that the $\zeta$ potential is defined at a special *surface of shear* or *slipping surface*, which is located somewhere in the diffuse layer, at a distance $s$ from the Stern layer. The exact position of the slipping surface is not known. It is widely accepted that this surface is located within a couple of molecular diameters (several angstroms) of the actual particle surface (52, 53). Correspondingly, the $\zeta$ potential is believed to be fairly close to the Stern potential $\psi_d$ in magnitude, and definitely less than the potential at the surface $\psi_0$ (53). Concerning the adsorption of surfactant counterions (like $DTA^+$) on a solid surface, one could write

$$\Gamma_1^{(\text{St})} < \Gamma_1^{(\zeta)} < \Gamma_1^{(\text{tot})}, \qquad [6.1]$$

where $\Gamma_1^{(\text{St})}$ denotes the surfactant ions belonging to the Stern layer (Fig. 1), $\Gamma_1^{(\zeta)}$ stands for the surfactant adsorption determined by $\zeta$-potential measurements, and $\Gamma_1^{(\zeta)}$ includes all surfactant ions confined between the slipping plane and the actual solid surface. $\Gamma_1^{(\text{tot})}$ is the total adsorption, defined by Eq. [1], which includes the surfactant ions in both Stern and diffuse layers. If $\zeta$ is fairly close to $\psi_d$, it follows that $\Gamma_1^{(\zeta)} \approx \Gamma_1^{(\text{St})} = \Gamma_1$, as assumed in the previous sections of this article. More precisely, Eq. [6.1] shows that the determined $\Gamma_1^{(\zeta)}$ can be considered an upper estimate for $\Gamma_1^{(\text{St})}$.

Saying "surfactant adsorption" one intuitively understands the ions immobilized in the Stern layer, that is $\Gamma_1^{(\text{St})}$. However, it

is worthwhile noting that all experimental methods, based on detecting a *depletion* of the bulk concentration (1–13), yield $\Gamma_1^{(\mathrm{tot})}$. Indeed, all depletion methods determine the background surfactant concentration, which excludes the ions involved in the particle counterion atmospheres; the latter incorporate both the Stern and diffuse layers.

Fortunately, one can determine $\Gamma_1^{(\mathrm{tot})}$ also from the $\zeta$-potential measurements (see below). This, in principle, allows one to compare the depletion and electrophoretic methods for measurement of surfactant adsorption at solid surfaces. With this end in view, one could express $\Gamma_1^{(\mathrm{tot})}$ in the form

$$\Gamma_1^{(\mathrm{tot})} = \Gamma_1^{(\zeta)} + \Delta\Gamma_1, \qquad [6.2]$$

where $\Delta\Gamma_1$ accounts for surfactant ions of the diffuse layer, which are located outside the slipping plane,

$$\Delta\Gamma_1 = c_{1\infty}\kappa^{-1}\int_0^\infty \left(\mathrm{e}^{\Phi(z)} - 1\right) dz, \qquad [6.3]$$

where $z = \kappa x$ is a dimensionless variable, $z = 0$ corresponds to the slipping plane, and $\Phi(z)$ is the magnitude of the dimensionless potential of the EDL. The latter is given by the Gouy–Chapman theory in the form (54)

$$\Phi(z) = 4\mathrm{arctanh}\left[\tanh(\tilde{\zeta}/4)\exp(-z)\right]. \qquad [6.4]$$

It is interesting to note that after substituting Eq. [6.4] into Eq. [6.3], the integration can be carried out analytically. The result reads

$$\Delta\Gamma_1 = 2c_{1\infty}\kappa^{-1}\lfloor\exp(\tilde{\zeta}/2) - 1\rfloor. \qquad [6.5]$$

As an example, in Fig. 9 we present the dependence $\Delta\Gamma_1(c_{1\infty})$, computed from Eq. [6.5], using the values of $\zeta$ and $c_{1\infty} = c_{1s}\exp(-\tilde{\zeta})$ from Fig. 5a, for the spherical glass particles. A comparison of Figs. 7 and 9 shows that in our case $\Delta\Gamma_1$ is much smaller than $\Gamma_1^{(\zeta)}$. In view of Eq. [6.2], this implies $\Gamma_1^{(\zeta)} \approx \Gamma_1^{(\mathrm{tot})}$.

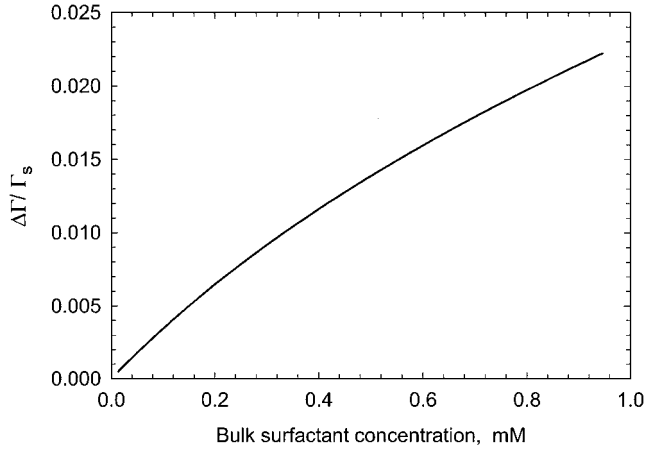


**FIG. 9.** Plot of $\Delta\Gamma_1$ vs the bulk surfactant concentration, $c_{1\infty}$, computed from Eq. [6.5] using values of $\zeta$ and $c_{1s}$ from Fig. 5a for the spherical glass particles.

The latter fact is not surprising insofar as in our experiments the surfactant concentration is much smaller than the total ionic strength ($c_{1\infty} \ll I$), which is due mainly to the added NaCl. In other words, the number of $DTA^+$ ions in the diffuse layer is much smaller than the number of $Na^+$ ions. For that reason, we may expect that the contribution of $DTA^+$ to $\Gamma_1^{(\mathrm{tot})}$ is due mostly to the binding of $DTA^+$ in the Stern layer; in such a case, the exact position of the slipping surface is not so crucial. In a future study we plan to verify the latter expectation, that is to check the coincidence of the values of $\Gamma_1^{(\mathrm{tot})}$ determined by independent depletion and $\zeta$-potential measurements. This will demand careful parallel experiments.

A second point of our discussion is the importance of the effect of *binding of inorganic counterions* (in our case $Na^+$) in the Stern layer. Note that the occupancy of the Stern layer can be greater than 70% for ionic strengths above 0.01 M (37). This effect markedly decreases the magnitudes of both $\psi_\mathrm{d}$ and $\zeta$ potentials (50), and it should be taken into account when interpreting measurements of adsorption and $\zeta$ potential, as is done in the present article. On the other hand, the neglecting of this effect could explain the unrealistically great distances, $s$, between the Stern and slipping planes estimated by some authors. For example, Kovačević *et al.* (10) determined the adsorption of salicylic acid on hematite particles using a depletion method. Comparing the computed $\psi_\mathrm{d}$ with the independently measured $\zeta$, the authors calculated $s = 15$ Å. The latter separation seems too large, because for the used ionic strength ($I = 0.228$ M, adjusted by NaCl) one has $\kappa^{-1} = 6.4$ Å. The account for the binding of $Na^+$ in the Stern layer would decrease the computed $|\psi_\mathrm{d}|$ and would lead to a smaller (realistic) calculated distance $s$. Similar approach could be applied to solve other pending problems about the $\psi_\mathrm{d}$ and $\zeta$ potentials, like that reported in Ref. (51).

## 7. SUMMARY AND CONCLUSIONS

In the present paper a method for determining the adsorption of surfactant on solid particles is proposed. It is based on processing data from $\zeta$-potential measurements by means of Eq. [12] (see Figs. 5a and 5b). From the fits of the data one obtains the adsorption constants (Table 3), which enable one to determine the surfactant and counterion adsorptions, $\Gamma_1$ and $\Gamma_2$, with the help of Eqs. [22]–[25] (see Figs. 7 and 8).

The method can be applied to particles of arbitrary size and shape, but only if their characteristic dimension is much larger than the thickness of the electric double layer, $\kappa^{-1}$. Remarkably, the adsorption of an ionic surfactant at a solid surface can be quantified by $\zeta$-potential experiments alone; additional measurements of concentration depletion and specific surface area of the particles are not needed. The proposed approach is suitable for the concentration range below the critical hemimicelle concentration, that is, in the ion exchange regime.

The method is applied to study the equilibrium adsorption of the cationic surfactant DTAB on glass particles in the presence of 1 mM NaBr. The particles are obtained by crushing a glass plate to powder and subsequent screening to remove all particles larger than 20 $\mu$m. The produced angular particles are shown in Fig. 2a. In some control experiments we used spherical particles (Fig. 2b) obtained by melting the angular ones in burning propane–butane (Fig. 3). The results for angular and spherical particles coincide in the framework of the experimental accuracy (see Table 3 and Figs. 7 and 8). As expected, the method is not sensitive to particle shape.

Since the surfactant ($DTA^+$) and $Na^+$ bear the same electric charge, they compete with each other in the adsorption on the negatively charged glass. This is taken into account in the theoretical model. The adsorption energy of a $DTA^+$ ion in the Stern layer is about 2.3 times greater than that of a $Na^+$ ion. For that reason, $DTA^+$ displaces $Na^+$ from the adsorption layer with the increase of the DTAB concentration. Thus the occupancy of the Stern layer with $Na^+$ decreases from 45% to 20% (Fig. 8). The latter facts imply that the presence of $Na^+$ ions in the Stern layer is always considerable and because of that they play an essential role in the overall adsorption process.

A future extension of the present study could involve obtaining a greater quantity of experimental results, measurements with other surfactants, and verification of the determined adsorptions against an independent method, say, the depletion one.

## ACKNOWLEDGMENTS

This work was supported by Colgate–Palmolive. The authors are indebted to Prof. Nikolai Denkov for the discussions and critical reading of the manuscript, and to Miss Nikolina Vassileva for obtaining the particle-size histogram (Fig. 4).

## REFERENCES

1. Krishnakumar, S., and Somasundaran, P., *Colloids Surf. A* **117,** 227 (1996).
2. Rehmet, R., and Killman, E., *Colloids Surf. A* **149,** 323 (1999).
3. Wang, W., and Kwak, J. C. T., *Colloids Surf. A* **156,** 95 (1999).
4. In, M., Bec, V., Aguerre-Chariol, O., and Zana, R., *Langmuir* **16,** 141 (2000).
5. Ivanova, N. I., Volchkova, I. L., and Shchukin, E. D., *Colloids Surf.* **101,** 239 (1995).
6. Zhao, J., and Brown, W., *J. Phys. Chem.* **100,** 3775 (1996).
7. Zhao, J., and Brown, W., *J. Phys. Chem.* **100,** 5908 (1996).
8. Alargova, R. G., Vakarelsky, I. Y., Paunov, V. N., Stoyanov, S. D., Kralchevsky, P. A., Mehreteab, A., and Broze, G., *Langmuir* **14,** 1996 (1998).
9. Dao, K., Bee, A., and Treiner, C., *J. Colloid Interface Sci.* **204,** 61 (1998).
10. Kovačević, D., Kallay, N., Antol, I., Pohlmeier, A., Lewandowski, H., and Narres, H. D., *Colloids Surf. A* **140,** 261 (1998).
11. Szekeres, M., Dékány, I., and de Keizer, A., *Colloids Surf. A* **141,** 327 (1998).
12. Nakashima, K., Yasuda, S., Nishihara, A., and Yamashita, Y., *Colloids Surf. A* **139,** 251 (1998).
13. Zhang, H., Penn, R. L., Hamers, R. J., and Banfield, J. F., *J. Phys. Chem. B* **103,** 4656 (1999).
14. Tiberg, F., Jonnson, B., Tang, J., and Lindman, B., *Langmuir* **10,** 2294 (1994).
15. Lee, E. M., Thomas, R. K., Cummins, P. G., Staples, E. J., Penfold, J., and Rennie, A. R., *Chem. Phys. Lett.* **162,** 196 (1989).
16. McDermott, D. C., Lu, J. R., Lee, E. M., Thomas, R. K., and Rennie, A. R., *Langmuir* **8,** 1204 (1992).
17. Li, Z. X., Weller, A., Thomas, R. K., Rennie, A. R., Webster, J. R. P., Penfold, J., Heenan, R. K., and Cubitt, R., *J. Phys. Chem. B* **103,** 10800 (1999).
18. Cummins, P. G., Staples, E., and Penfold, J., *J. Phys. Chem.* **94,** 3740 (1990).
19. Cummins, P. G., Staples, E., and Penfold, J., *J. Phys. Chem.* **95,** 5902 (1991).
20. Penfold, J., Staples, E., Tucker, I., and Cummins, P., *J. Phys. Chem.* **100,** 18133 (1996).
21. Nagashima, K., and Blum, F. D., *Colloids Surf. A* **176,** 17 (2001).
22. Bain, C. D., *Curr. Opin. Colloid Interface Sci.* **3,** 287 (1998).
23. Williams, C. T., Yong, Y., and Bain, C. D., *Langmuir* **16,** 2343 (2000).
24. Whitby, C. P., Scales, P. J., Grieser, F., Healy, T., Nishimura, S., and Tateyama, H., *J. Colloid Interface Sci.* **235,** 350 (2001).
25. Somasundaran, P., and Krishnakumar, S., *Colloids Surf. A* **123–124,** 491 (1997).
26. Scales, P. J., Grieser, F., and Healy, T. W., *Langmuir* **6,** 582 (1990).
27. Eremenko, B. V., Malysheva, M. L., Rusina, O. D., Kutsevol, N. V., and Zeltonozskaya, T. B., *Colloids Surf.* **98,** 19 (1995).
28. Nishimura, S., Scales, P. J., Biggs, S., Healy, T. W., *Langmuir* **16,** 690 (2000).
29. Gu, Y., and Li, D., *J. Colloid Interface Sci.* **226,** 328 (2000).
30. Mosquera, V., Ruso, J. M., Prieto, G., Sarmiento, F., *J. Phys. Chem.* **100,** 16749 (1996).
31. Dimov, N. K., Ahmed, E. H., Alargova, R. G., Kralchevsky, P. A., Durbut, P., Broze, G., and Mehreteab, A., *J. Colloid Interface Sci.* **224,** 116 (2000).
32. Somasundaran, P., and Fuerstenau, D. W., *J. Phys. Chem.* **70,** 90 (1966).
33. Stern, O., *Ztschr. Elektrochem.* **30,** 508 (1924).
34. Hachisu, S., *J. Colloid Interface Sci.* **33,** 445 (1970).
35. Hall, D. G., *in* "The Structure, Dynamics and Equilibrium Properties of Colloidal Systems" (D. M. Bloor and E. Wyn-Jones, Eds.), p. 857. Kluwer, Dordrecht, 1990.
36. Hall, D. G., *Colloids Surf. A* **90,** 285 (1994).
37. Kralchevsky, P. A., Danov, K. D., Broze, G., and Mehreteab, A., *Langmuir* **15,** 2351 (1999).
38. Aveyard, R., *in* "Surfactants" (Th.F. Tadros, Ed.), p. 153. Academic, London, 1984.
39. Somasundaran, P., and Krishnakumar, S., *Colloids Surf. A* **93,** 79 (1994).
40. Misselyn-Bauduin, A.-M., *in* "Handbook of Detergents. Part A: Properties" (G. Broze, Ed.), Ch. 6. Dekker, New York, 1999.
41. Prosser, A. J., and Franses, E. I., *Colloids Surf. A* **178,** 1 (2001).
42. Hill, T. L., "An Introduction to Statistical Thermodynamics." Addison-Wesley, Reading, MA, 1962.
43. Kirkwood, J. G., and Oppenheim, I., "Chemical Thermodynamics." McGraw-Hill, New York, 1961.
44. Frumkin, A., *Z. Physikal. Chem.* **116,** 466 (1925).
45. Langmuir, I., *J. Am. Chem. Soc.* **40,** 1361 (1918).
46. Davies, J. T., and Rideal, E. K., "Interfacial Phenomena." Academic, London, 1963.
47. Shchukin, E. D., Pertsov, A. V., Amelina, E. A., "Colloid Chemistry." Moscow Univ. Press, Moscow, 1982 (Russian); Elsevier, New York, 2001 (English).
48. Gouy, G., *J. Phys. Radium* **9,** 457 (1910).
49. Aveyard, R., Binks, B. P., Chen, J., Esquena, J., Fletcher, P. D. I., Buscall, R., Davies, S., *Langmuir* **14,** 4699 (1998).
50. Dukhin, S. S., "Electroconductivity and Electrokinetic Properties of Disperse Systems." Naukova Dumka, Kiev, 1975 (Russian).
51. Furusawa, K., Sasaki, H., Nashima, T., *in* "Electrical Phenomena at Interfaces" (H. Ohshima and K. Furusawa, Eds.), p. 225. Dekker, New York, 1998.
52. Hunter, R. J., "Zeta Potential in Colloid Science." Academic Press, London, 1981.
53. Hiemenz, P. C., Rajagopalan, R., "Principles of Colloid and Interface Science," 3rd ed., p. 541. Dekker, New York, 1997.
54. Overbeek, J. Th. G., *in* "Colloid Science," (H. R. Kruyt, Ed.), Vol. 1, p. 197. Elsevier, Amsterdam, 1952.